Combining the complex variable reproducing kernel particle method and the finite element method for solving transient heat conduction problems*

Chen Li(陈 丽)[a)b)], Ma He-Ping(马和平)[a)], and Cheng Yu-Min(程玉民)[c)†]

[a)] *Department of Mathematics, Shanghai University, Shanghai* 200072, *China*
[b)] *Department of Engineering Mechanics, Chang'an University, Xi'an* 710064, *China*
[c)] *Shanghai Institute of Applied Mathematics and Mechanics, Shanghai University, Shanghai* 200072, *China*

(Received 6 November 2012; revised manuscript received 19 December 2012)

In this paper, the complex variable reproducing kernel particle (CVRKP) method and the finite element (FE) method are combined as the CVRKP–FE method to solve transient heat conduction problems. The CVRKP–FE method not only conveniently imposes the essential boundary conditions, but also exploits the advantages of the individual methods while avoiding their disadvantages, then the computational efficiency is higher. A hybrid approximation function is applied to combine the CVRKP method with the FE method, and the traditional difference method for two-point boundary value problems is selected as the time discretization scheme. The corresponding formulations of the CVRKP–FE method are presented in detail. Several selected numerical examples of the transient heat conduction problems are presented to illustrate the performance of the CVRKP–FE method.

Keywords: complex variable reproducing kernel particle method, finite element method, combined method, transient heat conduction

PACS: 02.30.Fn, 02.30.Jr, 02.60.–x, 02.60.Cb **DOI:** 10.1088/1674-1056/22/5/050202

1. Introduction

Considerable research works have been carried out on transient heat transfer problems because they are closely related to many engineering applications,[1] such as electronic cooling, encapsulation, and cryogenics. However, due to complex material properties, boundary conditions, geometrical shapes, etc., it is usually very difficult to obtain the analytical solutions of these problems. Therefore, for many decades, considerable efforts have been made by researchers to develop various efficient numerical methods, such as the finite element (FE) method.[2] It is well known that the accuracy of the FE method relies on the quality of the mesh and the element type, and the mesh generation process consumes a lot of time for some problems, especially for discontinuous and high gradient problems.

To avoid the disadvantages of the FE method, meshless methods have attracted much attention in recent years due to the lack of dependence on the mesh, avoiding meshing, and ease of preparing the initial date.[3] Many meshless methods have been developed, including the element-free Galerkin (EFG) method,[4–6] the reproducing kernel particle (RKP) method,[7] the complex variable meshless method,[8–17] and meshless methods with boundary integral equations.[18–30]

The RKP method was originally introduced to improve the performance of the smoothed particle hydrodynamics (SPH) method in a finite domain by introducing a correction function to the kernel function of the integral transformation in the SPH method.[7] By imposing the reproducing conditions, the resulting modified kernel function reproduces polynomials exactly to a specific order and fulfills the completeness requirement. The RKP method not only shares the common features of all meshless methods but also has some unique features, such as time or space localization, hp-like adaptivity, and multi-resolution analysis.[31] All of these make the RKP method a novel approach for the studies of structural dynamics,[32,33] large deformation problems,[34,35] and fluid mechanics.[36]

Although the RKP method has lots of advantages over the other conventional numerical methods, it has a great computational cost, because a great number of nodes are selected in the domain of a problem, and the shape functions and their derivatives must be obtained at every node. Hence, the complex variable reproducing kernel particle (CVRKP) method was presented by the authors of this paper, and was then applied to two-dimensional elasticity, transient heat conduction problems, elastodynamics, and elasto-plasticity problems.[37–40] The advantage of the CVRKP method is that the correction function of a two-dimentional (2D) problem is formed with a one-dimentional (1D) basis function when the shape function is formed. Because the unknown coefficients of the correction function in the CVRKP approximation are fewer than

*Project supported by the National Natural Science Foundation of China (Grant No. 11171208) and the Special Fund for Basic Scientific Research of Central Colleges of Chang'an University, China (Grant No. CHD2011JC080).

†Corresponding author. E-mail: ymcheng@shu.edu.cn

© 2013 Chinese Physical Society and IOP Publishing Ltd

those in the RKP approximation, we need fewer nodes with support domains that cover an arbitrary point in the domain, and so fewer nodes are required in the whole domain of the problem without loss of the computational accuracy. Hence, the CVRKP method has greater precision and computational efficiency than the RKP method.

The disadvantages of the CVRKP method are listed as follows. (i) As the shape function of the CVRKP method does not satisfy the property of the Kronecker δ function, then the essential boundary conditions can not be applied directly. (ii) Compared to the FE method, the CVRKP method has a higher computational cost when constructing the shape functions and forming a global equation system, then it is expensive to apply the CVRKP method to solve those problems requiring a dense distribution of nodes over a large domain.

In this paper, the CVRKP and the FE methods are combined as the CVRKP–FE method to solve transient heat conduction problems. The CVRKP–FE method not only conveniently imposes the essential boundary conditions, but also exploits the advantages of the individual methods while avoiding their disadvantages, then the computational efficiency is higher. Several selected numerical examples of the transient heat conduction problems are presented to illustrate the performance of the CVRKP–FE method.

2. Combined techniques

Consider a two-dimensional transient heat conduction problem. The problem domain consists of two sub-domains $\Omega_{\rm F}$ and $\Omega_{\rm M}$ joined by an interface boundary $\Gamma_{\rm I}$, as shown in Fig. 1. The FE method is used in domain $\Omega_{\rm F}$, and the CVRKP method is used in domain $\Omega_{\rm M}$. In the CVRKP–FE method, the combination conditions on $\Gamma_{\rm I}$ must be satisfied.[41] But because the CVRKP shape functions do not satisfy the property of the Kronecker δ function, on the interface boundary $\Gamma_{\rm I}$, the nodal variables $T_{\rm I}^{\rm F}$ for $\Omega_{\rm F}$ differ from $T_{\rm I}^{\rm M}$ for $\Omega_{\rm M}$, i.e., $T_{\rm I}^{\rm F} \neq T_{\rm I}^{\rm M}$. It is thus impossible to couple the CVRKP and the FE methods directly along $\Gamma_{\rm I}$. In this paper, the hybrid approximation function is applied to satisfy the combination conditions by introducing interface elements between the FE and the CVRKP method domains. A detailed illustration of the interface domain is shown in Fig. 2. The $\Omega_{\rm I}$ is a sub-domain layer which is divided into several interface elements (finite elements) along interface boundary $\Gamma_{\rm I}$ within the meshless domain $\Omega_{\rm M}$. In these interface elements, a hybrid field variable approximation is defined to satisfy the field variable continuity across the interface boundaries. Before these interface elements are described in detail, the separate FE field variable interpolation and the CVRKP field variable approximations will be defined.

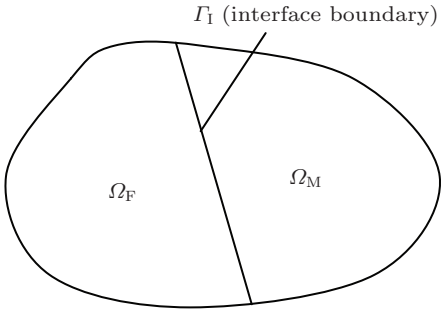


Fig. 1. Two sub-domains and the interface boundary in the CVRKP–FE method.

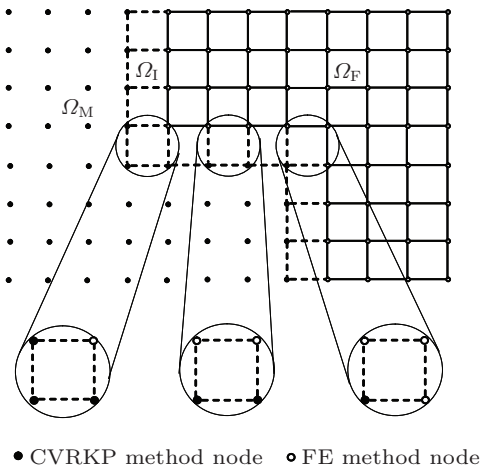


Fig. 2. Sub-domains used for FE–CVRKP coupling.

2.1. FE field variable interpolation function

The standard FE interpolation function for field variable $T(\boldsymbol{x},t)$ for an isoparametric element is

$$T^{\rm F}(\boldsymbol{x},t) = \sum_{I=1}^{n_{\rm F}} N_I(\boldsymbol{\zeta}(\boldsymbol{x}))T_I(t), \quad \boldsymbol{x} \in \Omega_{\rm F}, \tag{1}$$

where $n_{\rm F}$ is the node number of the element, N_I is the shape function, $T_I(t)$ is the nodal temperature at node $\boldsymbol{x}_I$, $\Omega_{\rm F}$ is the domain of the finite element, and $\boldsymbol{\zeta}(\boldsymbol{x}) = (\xi(\boldsymbol{x}), \eta(\boldsymbol{x}))$ is a mapping from the physical domain to the original domain.

2.2. CVRKP field variable approximation

The CVRKP method is used to construct the shape functions at scattered nodes in domain $\Omega_{\rm M}$. Because the field variable $T(z,t)$ of transient heat conduction problems is a scalar, the CVRKP approximation at an arbitrary point z is defined as

$$T^{\rm M}(z,t) = \sum_{I=1}^{n_{\rm M}} \tilde{\Phi}_I(z) \cdot T_I(t), \quad (z = x_1 + {\rm i}x_2 \in \Omega_{\rm M}), \tag{2}$$

where $n_{\rm M}$ is the total number of nodes in the support domain of point z, and $\tilde{\Phi}_I(z)$ is the shape function of the CVRKP method

$$\tilde{\Phi}_I(z) = {\rm Re}[\Phi_I(z)], \tag{3}$$

$$\Phi_I(z) = C(z; z - z_I) w_{\rm h}(z - z_I) \Delta V_I, \tag{4}$$

here $w_{\rm h}(z-z_I)$ is the weight function, ΔV_I is the volume of node I and represents the integration weight, and $C(z;z-z_I)$ is the correction function. In this study, the cubic spline function is chosen as the weight function. The correction function $C(z;z-z_I)$ is expressed as a linear combination of polynomial basis functions

$$C(z;z-z_I)=\sum_{i=0}^{N}p_i(z-z_I)b_i(z)=\boldsymbol{p}^{\rm T}(z-z_I)\boldsymbol{b}(z), \tag{5}$$

where N is the highest order of the polynomial basis functions, $p_i(z-z_I)$ are the basis functions, and $b_i(z)$ are the corresponding coefficients, which are obtained via the reproducing conditions

$$\boldsymbol{M}(z)\cdot\boldsymbol{b}(z)=\boldsymbol{H}, \tag{6}$$

with

$$\boldsymbol{M}(z)=\sum_{I=1}^{n}\boldsymbol{p}(z-z_I)\cdot\boldsymbol{p}^{\rm T}(z-z_I)\cdot w_{\rm h}(z-z_I)\cdot\Delta V_I, \tag{7}$$

$$\boldsymbol{H}=(1,0,\ldots,0)^{\rm T}. \tag{8}$$

From Eq. (6), we have

$$\boldsymbol{b}(z)=\boldsymbol{M}^{-1}(z)\cdot\boldsymbol{H}. \tag{9}$$

2.3. Interface field variable approximation

To illustrate the coupling procedure, we consider the coupling domain, as shown in Figs. 2 and 3. In domain $\Omega_{\rm M}$, the temperature $T(t)$ at an arbitrary point is approximated using the CVRKP method in Eq. (2), and in domain $\Omega_{\rm F}$, the FE interpolations in Eq. (1) are employed. In coupling domain Ω_I, the following expression is used:[41,42]

$$\begin{aligned}T^{\rm I}(\boldsymbol{x},t)\;=\;&\beta(\boldsymbol{x})\cdot T^{\rm M}(z(\boldsymbol{x}),t)+[1-\beta(\boldsymbol{x})]T^{\rm F}(\boldsymbol{x},t),\\&\boldsymbol{x}\in\Omega_{\rm I},\end{aligned} \tag{10}$$

where $T^{\rm I}(\boldsymbol{x},t)$ is the temperature approximation of a point in domain $\Omega_{\rm I}$; $T^{\rm M}(t)$ and $T^{\rm F}(t)$ are approximations for $T(\boldsymbol{x})$ in domain $\Omega_{\rm I}$ given by the CVRKP approximation and the FE interpolation, respectively; and $\beta(\boldsymbol{x})$ is a blending function. The $\beta(\boldsymbol{x})$ is constructed by using a linear ramp function

$$\beta(\boldsymbol{x})=3R^2(\boldsymbol{x})-2R^3(\boldsymbol{x}), \tag{11}$$

where $R(\boldsymbol{x})$ is a linear ramp function, which is defined using the shape functions of the FE method,[41] i.e.,

$$R(\boldsymbol{x})=\sum_{i=1}^{k}N_i(\boldsymbol{x}),\quad \boldsymbol{x}_i\in\Gamma_{\rm M}, \tag{12}$$

here k is the number of nodes located on meshless boundary $\Gamma_{\rm M}$ for an interface element. According to the property of the shape function of the FE method, $R(x)$ will be unity on meshless boundary $\Gamma_{\rm M}$ and vanish on boundary $\Gamma_{\rm F}$ ($\Gamma_{\rm I}$), which leads $\beta(\boldsymbol{x})$ to be unity on meshless boundary $\Gamma_{\rm M}$ and vanish on boundary $\Gamma_{\rm F}$, so the approximation $T^{\rm I}(\boldsymbol{x},t)$ will reduce to $T^{\rm M}(\boldsymbol{x},t)$ on $\Gamma_{\rm M}$ and $T^{\rm F}(\boldsymbol{x},t)$ on $\Gamma_{\rm F}$, thus ensuring the continuity.

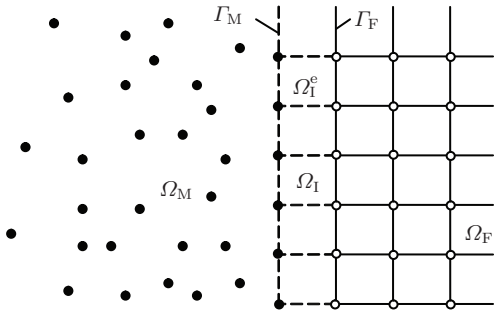


Fig. 3. Interface element used for FE–CVRKP coupling.

Substituting Eqs. (1) and (2) into Eq. (10), we can obtain the following interface shape function:

$$T^{\rm I}(\boldsymbol{x},t)=\sum_{I=1}^{n_{\rm M}}\bar{\Phi}_I(\boldsymbol{x})T_I(t),\quad \boldsymbol{x}\in\Omega_{\rm I}, \tag{13}$$

where $\bar{\Phi}_I(\boldsymbol{x})$ is the hybrid shape function of the interface element

$$\begin{aligned}\bar{\Phi}_I(\boldsymbol{x})\;=\;&\beta(\boldsymbol{x})\tilde{\Phi}_I(z)+[1-\beta(\boldsymbol{x})]N_I(\zeta(\boldsymbol{x})),\\&\boldsymbol{x}\in\Omega_{\rm I}.\end{aligned} \tag{14}$$

The derivatives of the interface shape function are

$$\begin{aligned}\bar{\Phi}_{I,j}(\boldsymbol{x})\;=\;&\beta(\boldsymbol{x})\tilde{\Phi}_{I,j}+\beta_{,j}(\boldsymbol{x})\tilde{\Phi}_I+[1-\beta(\boldsymbol{x})]N_{I,j}-\beta_{,j}(\boldsymbol{x})N_I,\\&\boldsymbol{x}\in\Omega_{\rm I},\end{aligned} \tag{15}$$

where

$$\beta_{,j}(\boldsymbol{x})=[6R(\boldsymbol{x})-6R^2(\boldsymbol{x})]R_{,j}, \tag{16}$$

$$R_{,j}(\boldsymbol{x})=\sum_{I=1}^{k}N_{I,j}(\zeta(\boldsymbol{x})),\quad \boldsymbol{x}\in\Gamma_{\rm M}. \tag{17}$$

This provides the continuous derivatives along the meshless boundary $\Gamma_{\rm M}$.

3. CVRKP–FE method for 2D transient heat conduction problems

The transient heat conduction equation is considered in this research as the canonical diffusion equation. The governing equation in a homogeneous, isotropic solid body occupying a closed domain Ω bounded by Γ is given by

$$\begin{aligned}&\rho c\cdot\frac{\partial T(\boldsymbol{x},t)}{\partial t}-\frac{\partial}{\partial x_1}\left(k_1\frac{\partial T(\boldsymbol{x},t)}{\partial x_1}\right)\\&-\frac{\partial}{\partial x_2}\left(k_2\frac{\partial T(\boldsymbol{x},t)}{\partial x_2}\right)-Q(\boldsymbol{x},t)=0\ \text{ in }\Omega,\end{aligned} \tag{18}$$

where $T(\boldsymbol{x},t)$ is the temperature field; t is time, k_1 and k_2 are the thermal conductivities of the material at x_1 and x_2 directions, respectively; ρ is the mass density, c is the specific heat

under a constant pressure, and $Q(\boldsymbol{x},t)$ is the density of body heat sources at internal point $\boldsymbol{x}$.

The problem domain Ω is enclosed by the total boundary Γ. The global boundary Γ consists of three parts, $\Gamma = \overset{3}{\underset{i=1}{\cup}} \Gamma_i$, and $\Gamma_i \cap \Gamma_j = \emptyset$ for $i \neq j$. The boundary conditions for this problem can be prescribed by any combination of the following types:

$$T(\boldsymbol{x},t) = \bar{T}(\boldsymbol{x},t) \ \text{ on } \Gamma_1, \tag{19}$$

$$k_1 \frac{\partial T(\boldsymbol{x},t)}{\partial x_1} n_1 - k_2 \frac{\partial T(\boldsymbol{x},t)}{\partial x_2} n_2 - \bar{q}(\boldsymbol{x},t) = 0 \ \text{ on } \Gamma_2, \tag{20}$$

$$k_1 \frac{\partial T(\boldsymbol{x},t)}{\partial x_1} n_1 - k_2 \frac{\partial T(\boldsymbol{x},t)}{\partial x_2} n_2 - h(T_\mathrm{a} - T(\boldsymbol{x},t)) = 0 \ \text{ on } \Gamma_3, \tag{21}$$

where $\bar{T}$, $\bar{q}$, and h are the prescribed temperatures, heat fluxes, and heat transfer coefficient on boundaries Γ_1, Γ_2, and Γ_3, respectively; n_1 and n_2 represent the vectors of unit outward normal to the global boundary; and T_a is the ambient temperature.

The initial condition is

$$T(\boldsymbol{x},t)|_{t=0} = T_0, \tag{22}$$

where T_0 is the initial temperature.

One of the aims for coupling the CVRKP and FE methods is to simplify the imposition of the essential boundary conditions, then the essential boundary should be included in the FE method domain. As both the FE and the CVRKP methods are discretized by using the Galerkin approximations, the weak forms can be used directly in the CVRKP–FE method without any modifications. The Galerkin weak form is

$$\int_\Omega \delta T \rho c \frac{\partial T}{\partial t} \mathrm{d}\Omega + \int_\Omega \delta (\boldsymbol{L}T)^\mathrm{T} \tilde{\boldsymbol{k}} (\boldsymbol{L}T) \mathrm{d}\Omega - \int_\Omega \delta T Q \mathrm{d}\Omega - \int_{\Gamma_2} \delta T \bar{q} \mathrm{d}\Gamma - \int_{\Gamma_3} \delta T h (T_\mathrm{a} - T) \mathrm{d}\Gamma = 0, \tag{23}$$

where

$$\boldsymbol{L} = \begin{bmatrix} \dfrac{\partial}{\partial x_1} \\ \dfrac{\partial}{\partial x_2} \end{bmatrix}, \tag{24}$$

$$\tilde{\boldsymbol{k}} = \begin{bmatrix} k_1 & 0 \\ 0 & k_2 \end{bmatrix}. \tag{25}$$

The weak form in Eq. (23) is used in the Galerkin procedure to develop the discrete equations. For transient heat conduction problems, the temperature at any point $\boldsymbol{x}$ is a function of the space coordinate and time t. In this paper, we first discretize the space domain at arbitrary time t. Because the shape functions are time independent, the node temperatures are only functions of time. Then we have

$$T^h(\boldsymbol{x},t) = \sum_{I=1}^n \hat{\Phi}_I(\boldsymbol{x}) T_I(t) = \hat{\boldsymbol{\Phi}}(\boldsymbol{x}) \cdot \boldsymbol{T}(t), \tag{26}$$

$$\frac{\partial T(\boldsymbol{x},t)}{\partial t} = \frac{\partial}{\partial t} \sum_{I=1}^n \hat{\Phi}_I(\boldsymbol{x}) T_I(t) = \sum_{I=1}^n \hat{\Phi}_I(\boldsymbol{x}) \frac{\partial T_I(t)}{\partial t} = \hat{\boldsymbol{\Phi}}(\boldsymbol{x}) \dot{\boldsymbol{T}}(t), \tag{27}$$

$$\boldsymbol{L}T^h(\boldsymbol{x},t) = \hat{\boldsymbol{B}}(\boldsymbol{x}) \cdot \boldsymbol{T}(t), \tag{28}$$

where

$$\boldsymbol{T}(t) = (T_1(t), T_2(t), \ldots, T_n(t))^\mathrm{T}, \tag{29}$$

$$\dot{\boldsymbol{T}}(t) = \left(\frac{\partial T_1(\boldsymbol{x},t)}{\partial t}, \frac{\partial T_2(\boldsymbol{x},t)}{\partial t}, \ldots, \frac{\partial T_n(\boldsymbol{x},t)}{\partial t} \right)^\mathrm{T}, \tag{30}$$

$$\hat{\boldsymbol{\Phi}} = \left(\hat{\Phi}_1(\boldsymbol{x}), \hat{\Phi}_2(\boldsymbol{x}), \ldots, \hat{\Phi}_n(\boldsymbol{x}) \right), \tag{31}$$

$$\hat{\Phi}_I(\boldsymbol{x}) = \begin{cases} N_I(\boldsymbol{\zeta}(\boldsymbol{x})), & \boldsymbol{x} \in \Omega_\mathrm{F}, \\ \tilde{\Phi}_I(z(\boldsymbol{x})), & \boldsymbol{x} \in \Omega_\mathrm{M}, \\ \bar{\Phi}_I(\boldsymbol{x}), & \boldsymbol{x} \in \Omega_\mathrm{I}, \end{cases} \tag{32}$$

$$\hat{\boldsymbol{B}}(\boldsymbol{x}) = \left(\hat{\boldsymbol{B}}_1(\boldsymbol{x}), \hat{\boldsymbol{B}}_2(\boldsymbol{x}), \ldots, \hat{\boldsymbol{B}}_n(\boldsymbol{x}) \right), \tag{33}$$

$$\hat{\boldsymbol{B}}_I(\boldsymbol{x}) = \begin{cases} \boldsymbol{B}_I^\mathrm{F}(\boldsymbol{\zeta}(\boldsymbol{x})), & \boldsymbol{x} \in \Omega_\mathrm{F}, \\ \boldsymbol{B}_I^\mathrm{M}(z(\boldsymbol{x})), & \boldsymbol{x} \in \Omega_\mathrm{M}, \\ \boldsymbol{B}_I^\mathrm{I}(\boldsymbol{x}), & \boldsymbol{x} \in \Omega_\mathrm{I}, \end{cases} \tag{34}$$

$$\boldsymbol{B}_I^\mathrm{F}(\boldsymbol{x}) = \begin{bmatrix} N_{I,1}(\boldsymbol{\zeta}(\boldsymbol{x})) \\ N_{I,2}(\boldsymbol{\zeta}(\boldsymbol{x})) \end{bmatrix}, \tag{35}$$

$$\boldsymbol{B}_I^\mathrm{M}(z) = \begin{bmatrix} \tilde{\Phi}_{I,1}(z) \\ \tilde{\Phi}_{I,2}(z) \end{bmatrix}, \tag{36}$$

$$\boldsymbol{B}_I^\mathrm{I}(\boldsymbol{x}) = \begin{bmatrix} \bar{\Phi}_{I,1}(\boldsymbol{x}) \\ \bar{\Phi}_{I,2}(\boldsymbol{x}) \end{bmatrix}. \tag{37}$$

Substituting Eqs. (26)–(28) into Eq. (23) yields

$$\begin{aligned} &\int_\Omega \delta \left(\hat{\boldsymbol{\Phi}}(z)\boldsymbol{T} \right)^\mathrm{T} \cdot \rho c \cdot \left(\hat{\boldsymbol{\Phi}}(z)\dot{\boldsymbol{T}} \right) \mathrm{d}\Omega \\ &+ \int_\Omega \delta \left(\hat{\boldsymbol{B}}(z)\boldsymbol{T} \right)^\mathrm{T} \tilde{\boldsymbol{k}} \left(\hat{\boldsymbol{B}}(z)\boldsymbol{T} \right) \mathrm{d}\Omega \\ &- \int_\Omega \delta \left(\hat{\boldsymbol{\Phi}}(z)\boldsymbol{T} \right)^\mathrm{T} \cdot Q \mathrm{d}\Omega - \int_{\Gamma_2} \delta \left(\hat{\boldsymbol{\Phi}}(z)\boldsymbol{T} \right)^\mathrm{T} \cdot \bar{q} \mathrm{d}\Gamma \\ &- \int_{\Gamma_3} \delta \left(\hat{\boldsymbol{\Phi}}(z)\boldsymbol{T} \right)^\mathrm{T} \cdot h \cdot T_\mathrm{a} \mathrm{d}\Gamma \\ &+ \int_{\Gamma_3} \delta \left(\hat{\boldsymbol{\Phi}}(z)\boldsymbol{T} \right)^\mathrm{T} \cdot h \cdot \left(\hat{\boldsymbol{\Phi}}(z)\boldsymbol{T} \right) \mathrm{d}\Gamma = 0. \end{aligned} \tag{38}$$

The nodal test function values $\delta \boldsymbol{T}^\mathrm{T}$ are arbitrary, then we have the following discrete equation:

$$\boldsymbol{C}\dot{\boldsymbol{T}} + \bar{\boldsymbol{K}}\boldsymbol{T} = \bar{\boldsymbol{F}}, \tag{39}$$

$$\bar{\boldsymbol{K}} = \boldsymbol{K} + \boldsymbol{H}, \tag{40}$$

$$\bar{\boldsymbol{F}} = \boldsymbol{F}^{(1)} + \boldsymbol{F}^{(2)} + \boldsymbol{F}^{(3)}, \tag{41}$$

where

$$C_{IJ} = \int_\Omega \hat{\Phi}_I(\boldsymbol{x}) \cdot \rho c \cdot \hat{\Phi}_J(\boldsymbol{x}) \mathrm{d}\Omega, \tag{42}$$

$$K_{IJ} = \int_\Omega \hat{\boldsymbol{B}}_I^\mathrm{T}(\boldsymbol{x}) \cdot \tilde{\boldsymbol{k}} \cdot \hat{\boldsymbol{B}}_J(\boldsymbol{x}) \mathrm{d}\Omega, \tag{43}$$

$$H_{IJ} = \int_{\Gamma_3} \hat{\Phi}_I(\boldsymbol{x}) \cdot h \cdot \hat{\Phi}_J(\boldsymbol{x}) \mathrm{d}\Gamma, \tag{44}$$

$$f_I^{(1)} = \int_\Omega \hat{\Phi}_I(\boldsymbol{x}) \cdot Q \mathrm{d}\Omega, \tag{45}$$

$$f_I^{(2)} = \int_{\Gamma_2} \hat{\Phi}_I(\boldsymbol{x}) \cdot \bar{q} \mathrm{d}\Gamma, \tag{46}$$

$$f_I^{(2)} = \int_{\Gamma_3} \hat{\Phi}_I(\boldsymbol{x}) \cdot h \cdot T_a \, \mathrm{d}\Gamma. \tag{47}$$

The simulation of a complex transient heat conduction problem requires a high efficient technique for the time discretization. In this paper, the traditional difference method for two-point boundary value problems is applied to discretize the time-dependent term in Eq. (39). Then we have

$$\left(\frac{\boldsymbol{C}}{\Delta t} + \theta \bar{\boldsymbol{K}}_{t+\Delta t}\right) \boldsymbol{T}_{t+\Delta t} = \left(\frac{\boldsymbol{C}}{\Delta t} - (1-\theta)\bar{\boldsymbol{K}}_t\right) \boldsymbol{T}_t + \theta \bar{\boldsymbol{F}}_{t+\Delta t} + (1-\theta)\bar{\boldsymbol{F}}_t, \tag{48}$$

where θ is a parameter related to the precision. In this paper, the classical Galerkin form is adopted, then $\theta = 2/3$. The time domain will be discretized by n time increments. We assume that the analysis starts at time t and the temperature T_t is known, then we will obtain $T_{t+\Delta t}$.

4. Numerical examples

In this section, numerical results for selected examples are presented to illustrate the applicability of the proposed CVRKP–FE method.

In the numerical examples presented in this section, a regular arrangement of nodes and the background mesh of cells are used for the numerical integrations to calculate the system equation. A 4×4 Gaussian quadrature is used for the integration. The linear basis and the cubic spline weight function are used in the CVRKP approximation.

4.1. Convergence analysis and error estimation

The convergence study of the present CVRKP–FE method on the 2D transient heat conduction problems is carried out by analyzing the final node temperatures under different discretization schemes and different scaling factors $d_{\max}$. The scaling factor is a measure of the size of the support domain of the weight function. For the purpose of error estimation and convergence studies, the Sobolev norms

$$\|T\|_0 = \left(\int_\Omega T^2 \, \mathrm{d}\Omega\right)^{1/2}, \tag{49}$$

$$\|T\|_1 = \left(\int_\Omega T^2 + (|\nabla T|)^2 \, \mathrm{d}\Omega\right)^{1/2} \tag{50}$$

are considered. And the relative errors are defined as

$$r_k = \frac{\|T^{\mathrm{num}} - T^{\mathrm{exact}}\|_k}{\|T^{\mathrm{exact}}\|_k}, \quad k = 0, 1. \tag{51}$$

We apply the present method to the 2D heat conduction problem with mixed boundary conditions on a rectangular domain. The governing equation is

$$\frac{\partial T}{\partial t} - \frac{\partial^2 T}{\partial x_1^2} - \frac{\partial^2 T}{\partial x_2^2} = 0,$$

$$0 < x_1 < \pi, \ \ 0 < x_2 < \pi, \ \ t \geq 0, \tag{52}$$

the boundary conditions are

$$\frac{\partial T}{\partial x_1}(0, x_2, t) = \frac{\partial T}{\partial x_1}(\pi, x_2, t) = 0, \tag{53}$$

$$T(x_1, 0, t) = T(x_1, \pi, t) = 0, \tag{54}$$

and the initial condition is

$$T(x_1, x_2, 0) = \cos x_1 \sin x_2 + \cos(2x_1)\sin(2x_2), \tag{55}$$

where $T = T(x_1, x_2, t)$ is the temperature of any point located at position (x_1, x_2) of a rectangular plate at time t.

The analytical solution is

$$T(x_1, x_2, t) = \mathrm{e}^{-2t} \cos x_1 \sin x_2 + \mathrm{e}^{-8t} \cos 2x_1 \sin 2x_2. \tag{56}$$

In the computation, the time step chosen for the integration is $\Delta t = 0.001$ s. It is known that the choice of scaling factors d_{max} has an influence on the support domain of nodes within the meshless domain Ω_{M}, and further influences the performance of the present CVRKP–FE method. Therefore, the influences of scaling factors $d_{\max}$ on the numerical results are studied firstly, where different regular nodal distributions are used. The relation between the relative error norms and scaling factors $d_{\max}$ is plotted in Fig. 4. From the numerical result, we observe that it is a good choice to take $d_{\max} = 1.3$–1.4. With the above analysis, $d_{\max} = 1.4$ is taken in the following 2D transient heat conduction examples.

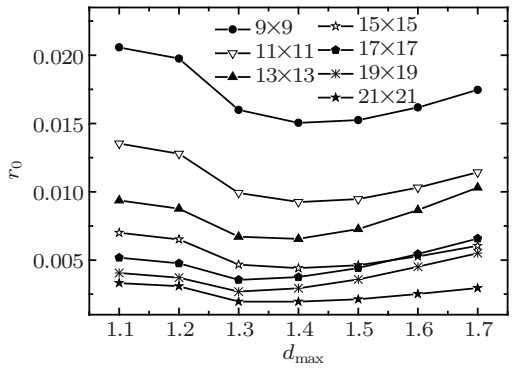


Fig. 4. Influence of parameter $d_{\max}$ on the relative error r_0.

Regular node distributions of 9×9, 15×15, and 21×21 are used to study the convergence of the present CVRKP–FE method. The size h in the figure is defined as the distance in the x_1 direction between two neighbor nodes with the same x_2 coordinate. The relative errors and the convergence rates for norms $\|\cdot\|_0$ and $\|\cdot\|_1$ for the present CVRKP–FE method, the CVRKP method, and the FE method with mesh refinement are shown in Figs. 5 and 6, respectively. It can be seen that the present method has high rates of convergence for norms $\|\cdot\|_0$ and $\|\cdot\|_1$, and gives reasonably accurate results for the unknown variable and its derivatives.

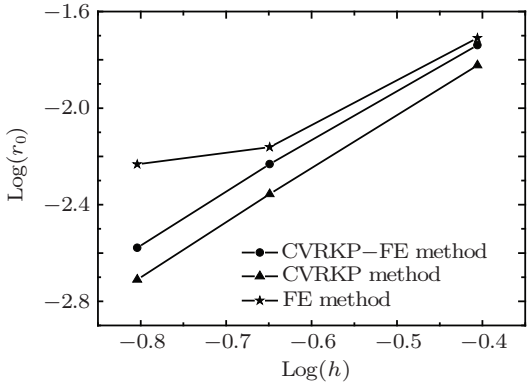


Fig. 5. Relative errors and convergence rates for norm $\|\cdot\|_0$.

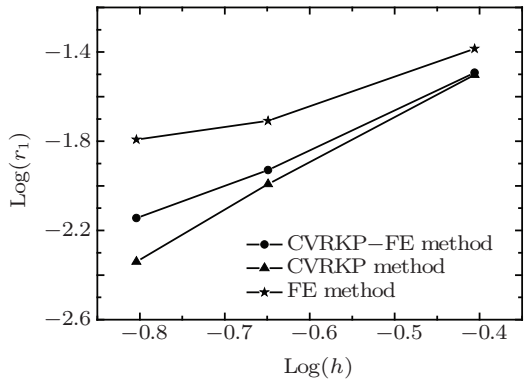


Fig. 6. Relative errors and convergence rates for norm $\|\cdot\|_1$.

The computational errors in the present CVRKP–FE method are compared with those in the FE and the CVRKP methods, as shown in Fig. 7. It can be observed that the computational accuracy of the present CVRKP–FE method is higher than that of the conventional FE method under the same node distribution. Moreover when the number of nodes increases, the results obtained by the present CVRKP–FE method become more accurate.

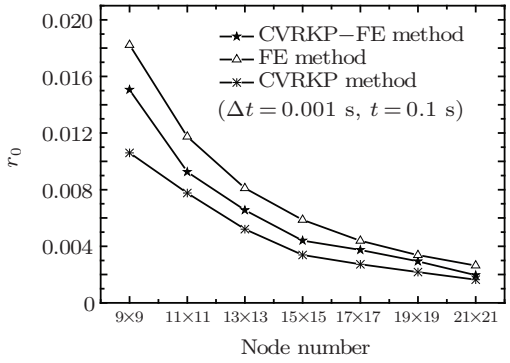


Fig. 7. Relationship between the number of nodes and the relative error r_0.

Table 1 shows that for the similar relative error, the proposed CVRKP–FE method takes less CPU time compared with the CVRKP method.

Table 1. Comparison of the CPU time for the example ($\Delta t = 0.001$ s).

Time/s	CVRKP–FE method/s	CVRKP method/s	FE method/s
0.1	2.469	2.985	0.781
0.3	2.859	3.469	1.047
0.5	3.235	3.828	1.360
0.7	3.609	4.266	1.547
0.9	3.937	4.781	1.782
1.1	4.313	5.329	2.063

4.2. The 2D heat conduction with Dirichlet boundary conditions

We apply the present CVRKP–FE method to the following 2D inhomogeneous heat conduction problem with Dirichlet boundary conditions on a rectangular domain. The governing equation is

$$\frac{\partial T}{\partial t} - \frac{\partial^2 T}{\partial x_1^2} - \frac{\partial^2 T}{\partial x_2^2} = 0, \quad x_1, x_2 \in (0,1), \quad t \geq 0, \tag{57}$$

the boundary conditions are

$$T(0, x_2, t) = \mathrm{e}^{-2t} \sin(x_2), \tag{58}$$

$$T(1, x_2, t) = \mathrm{e}^{-2t} \sin(1 + x_2), \tag{59}$$

$$T(x_1, 0, t) = \mathrm{e}^{-2t} \sin(x_1), \tag{60}$$

$$T(x_1, 1, t) = \mathrm{e}^{-2t} \sin(1 + x_1), \tag{61}$$

and the initial condition is

$$T(x_1, x_2, 0) = \sin(x_1 + x_2). \tag{62}$$

The analytical solution is

$$T(x_1, x_2, t) = \mathrm{e}^{-2t} \sin(x_1 + x_2). \tag{63}$$

In this example, the regular node distribution of 21×21 is used for the present CVRKP–FE method, as shown in Fig. 8. The time step $\Delta t = 0.001$ s is chosen for the integration. In addition, based on the results of the previous numerical example, we take the scaling factor $d_{\max} = 1.4$. The variations of the temperatures at x_1 and x_2 directions at five different time are shown in Figs. 9 and 10, respectively. It can be seen that there is an excellent agreement between the present CVRKP–FE method and the analytical results.

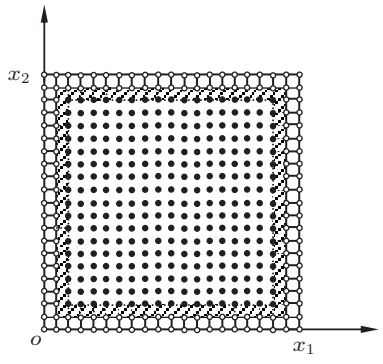


Fig. 8. Nodes and mesh arrangement. The shaded elements are those adjacent to the interface of the FE method domain (outside) and the CVRKP method domain (inside).

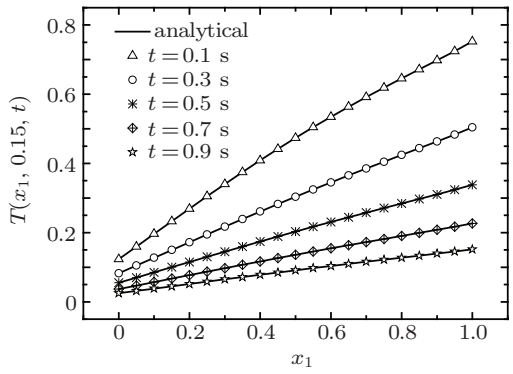


Fig. 9. Temperature variation at x_1 direction at different time.

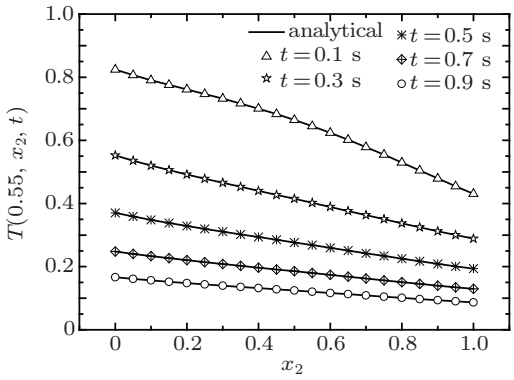


Fig. 10. Temperature variation with x_2 coordinate at different time.

4.3. The 2D inhomogeneous heat conduction with Dirichlet boundary conditions

The governing equation is

$$\frac{\partial T}{\partial t} - \frac{\partial^2 T}{\partial x_1^2} - \frac{\partial^2 T}{\partial x_2^2} = \left(1+t^2\right) T + \left(2\pi^2 - t^2 - 2\right) \mathrm{e}^{-t} \sin(\pi x_1) \cos(\pi x_2), \quad x_1,\, x_2 \in (0,1),\ t \geq 0, \tag{64}$$

the boundary conditions are

$$T(0, x_2, t) = T(1, x_2, t) = 0, \tag{65}$$

$$T(x_1, 0, t) = -T(x_1, 1, t) = \mathrm{e}^{-t} \sin(\pi x_1), \tag{66}$$

and the initial condition is

$$T(x_1, x_2, 0) = \sin(\pi x_1) \cos(\pi x_2). \tag{67}$$

The analytical solution is

$$T(x_1, x_2, t) = \mathrm{e}^{-t} \sin(\pi x_1) \cos(\pi x_2). \tag{68}$$

In this study, the scaling factor $d_{\max} = 1.4$ and the time step $\Delta t = 0.001$ s are used for the present CVRKP–FE method. The node distribution of 11×11 is shown in Fig. 11.

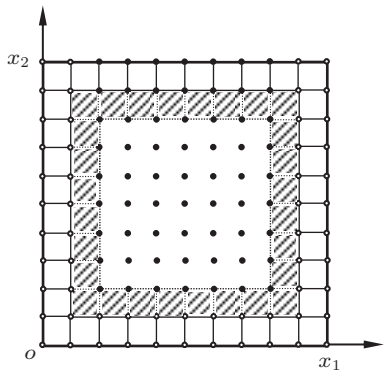


Fig. 11. Nodes and mesh arrangement.

The analytical solution and the results of the present CVRKP–FE method at $(x_1,\ 0.6)$ and $(0.4, x_2)$ are plotted with time (see Figs. 12 and 13). It can be observed that the numerical results are in very good agreement with the analytical solution. Figures 14 and 15 plot the analytical solution and the numerical solutions obtained using the present CVRKP–FE method, the CVRKP method, and the FE method at x_1 and x_2 directions, respectively. It can be observed that both the present CVRKP–FE method and the CVRKP method give very similar results for the entire domain, but compared with the CVRKP method, the proposed CVRKP–FE method takes less CPU time. Moreover, it is again shown that the present CVRKP–FE method has higher computational precision than the FE method.

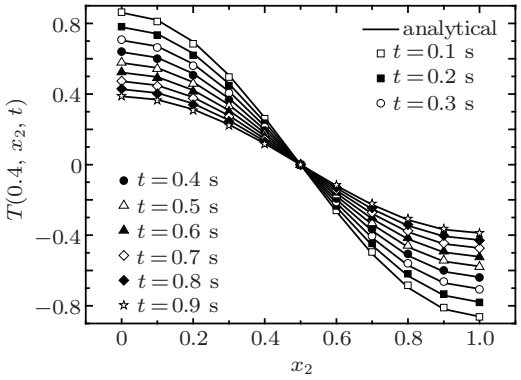


Fig. 12. Temperature distributions at x_2 direction when $x_1 = 0.4$.

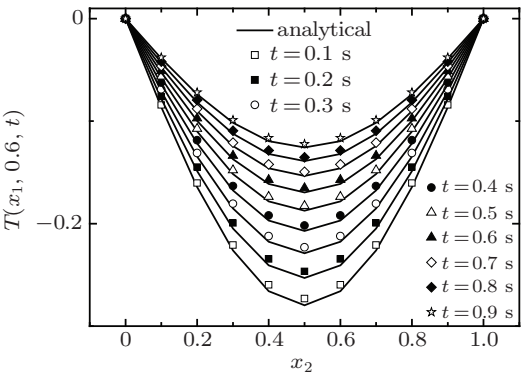


Fig. 13. Temperature distributions at x_1 direction when $x_2 = 0.6$.

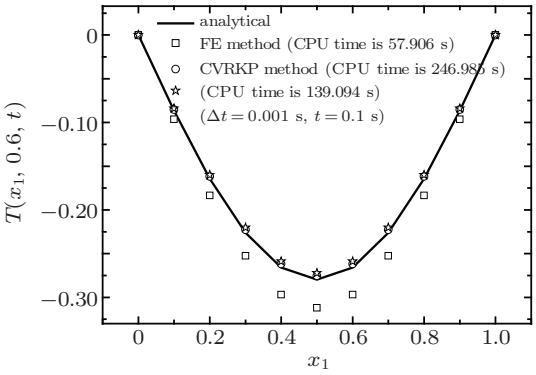


Fig. 14. Comparison of the temperature distributions when $x_2 = 0.6$.

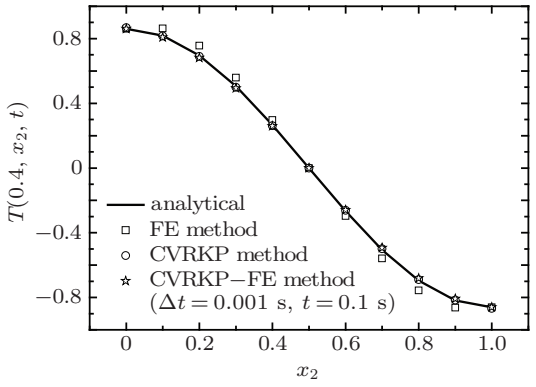


Fig. 15. Comparison of the temperature distributions when $x_1 = 0.4$.

5. Conclusion

We have discussed the coupling of the CVRKP and the FE methods for transient heat conduction problems. Several numerical examples are presented to verify the accuracy of the numerical formulations, with the results indicating that the CVRKP–FE method can effectively reduce the computational cost of the solution with no adverse effect on the accuracy. The computational cost is lower because the difficulty of imposing the essential boundary conditions for the CVRKP method can be overcome by modeling the portion of the domain with the essential boundaries using the FE method, which uses the shape function with the Kronecker δ function property. Hence, the boundary conditions are treated directly, as in the FE method. A comparison of the results of the CVRKP–FE method and the corresponding analytical solutions demonstrates that the CVRKP–FE method is both feasible and effective.

References

[1] Lewis R W, Morgan K, Thomas H R and Seetharamu K N 1996 *The Finite Element Method in Heat Transfer Analysis* (Chichester: Wiley)
[2] Bathe K J and Khoshgoftar M R 1979 *Nucl. Eng. Des.* **51** 389
[3] Belytschko T, Krongauz Y, Organ D, Fleming M and Krysl P 1996 *Comput. Meth. Appl. Mech. Eng.* **139** 3
[4] Belytschko T, Lu Y Y and Gu L 1994 *Int. J. Numer. Meth. Eng.* **37** 229
[5] Cheng R J and Cheng Y M 2008 *Acta Phys. Sin.* **57** 6037 (in Chinese)
[6] Cheng R J and Cheng Y M 2011 *Chin. Phys. B* **20** 070206
[7] Liu W K, Jun S and Zhang Y F 1995 *Int. J. Numer. Meth. Fluids* **20** 1081
[8] Cheng Y M and Li J H 2005 *Acta Phys. Sin.* **54** 4463 (in Chinese)
[9] Cheng Y M and Li J H 2006 *Sci. China G: Phys. Mech. Astron.* **49** 46
[10] Liew K M, Feng C, Cheng Y M and Kitipornchai S 2007 *Int. J. Numer. Meth. Eng.* **70** 46
[11] Peng M J, Li D M and Cheng Y M 2011 *Engineering Structures* **33** 127
[12] Liew K M and Cheng Y M 2009 *Comput. Meth. Appl. Mech. Eng.* **198** 3925
[13] Bai F N, Li D M, Wang J F and Cheng Y M 2012 *Chin. Phys. B* **21** 020204
[14] Li D M, Bai F N, Cheng Y M and Liew K M 2012 *Comput. Meth. Appl. Mech. Eng.* **233–236** 1
[15] Ren H P and Cheng Y M 2012 *International Journal of Computational Materials Science and Engineering* **1** 1250011
[16] Cheng Y M, Wang J F and Bai F N 2012 *Chin. Phys. B* **21** 090203
[17] Cheng Y M, Li R X and Peng M J 2012 *Chin. Phys. B* **21** 090205
[18] Zhu T, Zhang J D and Atluri S N 1999 *Eng. Anal. Bound. Elem.* **23** 375
[19] Sun Y Z, Zhang Z, Kitipornchai S and Liew K M 2006 *International Journal of Engineering Science* **44** 37
[20] Kothnur V S, Mukherjee S and Mukherjee Y X 1999 *Journal of Solids and Structures* **36** 1129
[21] Liew K M, Cheng Y M and Kitipornchai S 2006 *Int. J. Numer. Meth. Eng.* **65** 1310
[22] Kitipornchai S, Liew K M and Cheng Y M 2005 *Comput. Mech.* **36** 13
[23] Cheng Y M and Peng M J 2005 *Sci. China G: Phys. Mech. Astron.* **48** 641
[24] Liew K M, Cheng Y M and Kitipornchai S 2005 *Int. J. Numer. Meth. Eng.* **64** 1610
[25] Liew K M, Cheng Y M and Kitipornchai S 2007 *Int. J. Solids Struct.* **44** 4220
[26] Qin Y X and Cheng Y M 2006 *Acta Phys. Sin.* **55** 3215 (in Chinese)
[27] Dai B D and Cheng Y M 2007 *Acta Phys. Sin.* **56** 597 (in Chinese)
[28] Peng M J and Cheng Y M 2009 *Eng. Anal. Bound. Elem.* **33** 77
[29] Cheng Y M, Liew K M and Kitipornchai S 2009 *Int. J. Numer. Meth. Eng.* **78** 1258
[30] Ren H P and Zhang W 2009 *Chin. Phys. B* **18** 4065
[31] Liu W K, Chen Y, Jun S, Chen J S and Belytschko T 1996 *Archives of Computer Methods in Engineering State of the Art Review* **3** 3
[32] Liu W K, Jun S, Li S, Adee J and Belytschko T 1995 *Int. J. Numer. Meth. Eng.* **38** 1655
[33] Liew K M, Ng T Y, Zhao X and Reddy J N 2002 *Comput. Meth. Appl. Mech. Eng.* **191** 4141
[34] Chen J S, Chen C, Wu C T and Liu W K 1996 *Comput. Meth. Appl. Mech. Eng.* **139** 195
[35] Liu W K and Jun S 1998 *Int. J. Numer. Meth. Eng.* **41** 1339
[36] Liu W K, Jun S, Thomas S D, Chen Y and Hao W 1997 *Int. J. Numer. Meth. Fluids* **24** 1391
[37] Chen L and Cheng Y M 2008 *Acta Phys. Sin.* **57** 1 (in Chinese)
[38] Chen L and Cheng Y M 2008 *Acta Phys. Sin.* **57** 6047 (in Chinese)
[39] Chen L and Cheng Y M 2010 *Chin. Phys. B* **19** 090204
[40] Chen L and Cheng Y M 2010 *China G: Phys. Mech. Astron.* **53** 954
[41] Belytschko T and Organ D 1995 *Comput. Mech.* **17** 186
[42] Dolbow J and Belytschko T 1999 *Int. J. Numer. Meth. Eng.* **46** 925